TAO, Vol. 7, No. 3, 257-268, September 1996

SH Wave Seismogram Synthesis by the Finite Element Method

Bor-Shouh Huang[1]

(Manuscript received 14 December 1995, in final form 20 March 1996)

ABSTRACT

A method for the finite element computation of the synthetic seismograms of SH wave propagation in a two-dimensional (2-D) medium is proposed. The finite element method has the advantage of specifying the arbitrary density and velocity field in the medium. To complete the waveform modeling for an earthquake, the transformation of line source snapshots and seismograms of the 2-D finite element modeling to the point source responses is critically necessary. The accuracy of the finite element modeling is verified by comparing it with the generalized ray method and with a finite difference method which computes the 2-D wave field from a different approach. The aim of this study is to demonstrate the successfulness of seismogram synthesis by the finite element method and to propose the potential applications of this method in the Taiwan area.

(Key words: SH wave, Finite element method, Seismogram synthesis, 2-D modeling)

1. INTRODUCTION

Wave propagation problems in complicated geological structures have generated considerable interests in recent years. The full wave equation modeling with numerical methods such as the finite differences (FD), the finite element (FE) and the pseudo-spectrum (PS) methods is a suitable approach. However, modeling wave propagation with three-dimensional (3-D) structures is, in fact, difficult to handle with present-day computers. These methods require a tremendous amount of computer time and also allow only a limited number of wavelengths to propagate. From this point of view, 2-D modeling is more practical to use. The application of 2-D modeling has been proposed in many problems of seismological interest (Aki and Larner, 1970; Dravinski, 1983). However, the Green's function of 2-D (line source) is actually different to that of 3-D (point source), so application is limited to earthquake waveform synthesis, such as the generalized ray theory (GRT) method (Heaton and Helmberger, 1977), WKBJ method (Chapman, 1978) and the frequency-wavenumber (FK) method (Wang and Herrmann, 1980). Recently, Vidale *et al.* (1985) proposed a new approach to seismic wave propagation modeling including laterally varying structures with the 2-D FD scheme and applying it to waveform synthesis.

[1]Institute of Earth Sciences, Academia Sinica, P. O. Box 1-55, Nankang, Taipei, Taiwan, R.O.C.

They generated the seismic waves in source area by the GRT and computed the wave propagation by the 2-D FD method. Finally, they calibrated the propagated energy from 2-D to 3-D by a suitable transformation discussed below. This approach is successful in computing a 3-D wavefield for a 2-D lateral heterogeneous model and is widely applied to ground motion simulation (Vidale *et al.*, 1985; Ho-Liu and Helmberger, 1989). In this study, a new FE approach to model the 2-D Green's functions based on equivalent body forces is proposed. The couples that were required to obtain equivalent forces for a generally oriented displacement discontinuity (Aki and Richards, 1980) were directly implemented. This simplified the numerical computation for dislocation sources. The obtained Green's functions were easy to modify for the linear moment tensor inversions algorithms (Stump and Johnson, 1977; Kikuchi and Kanamori, 1991; Huang, 1994). Furthermore, a numerical technique of computing convolution on grid points of the 2-D model is proposed to simulate the point source wavefield snapshots, which have not been discussed before.

2. METHOD

2.1 The Representation of the 2-D and 3-D Green's Functions

The 3-D point source, scalar wave equation can be written as:

$$\left[\nabla_3^2 - \frac{1}{c^2}\right] G_3(x,y,z,t) = -\delta(x)\delta(y)\delta(z)\delta(t), \tag{1}$$

where G_3 is the 3-D Green's function, δ(t) is the Dirac delta function and ∇_3 is the 3-D Laplacian operator in Cartesian coordinates. The wave speed c in equation (1) may be an arbitrary function of spatial coordinates, i.e., $c(x,y,z)$. For constant c, the solution of equation (1) is:

$$G_3(x,y,z,t) = \frac{\delta(t - r/c)}{4\pi r}; \qquad r = \sqrt{x^2 + y^2 + z^2}. \tag{2}$$

The significant properties of G_3 are: (1) its amplitude decays (geometric spreading) as 1/r, and (2) its propagating waveform is identical to the source pulse.

Corresponding to the 3-D wave equation, the 2-D wave equation is

$$\left[\nabla_2^2 - \frac{1}{c^2}\right] G_2(x,z,t) = -\delta(x)\delta(z)\delta(t), \tag{3}$$

where G_2 is the 2-D Green's function and ∇_2 is the 2-D Laplacian operator. Physically, equation (3) describes a wavefield emanated from a point source in space with coordinates x and z, which are equivalent to a line source along the y-axis in space with coordinates x, y and z. The same conditions hold as in the 3-D case discussed above. Thus, the 2-D Green's function has the following form:

$$G_2(x,z,t) = \frac{H(t - r/c)}{4\pi r}; \qquad r = \sqrt{x^2 + z^2}, \tag{4}$$

where H(t) is the Heaviside step function. The features of G_2 are: (1) its amplitude decays as $1/(\sqrt{r})$, (2) its propagating waveform is different from the source pulse and includes a low decay tail. The differences between the 2-D and 3-D Green's functions are shown in Figure 1.

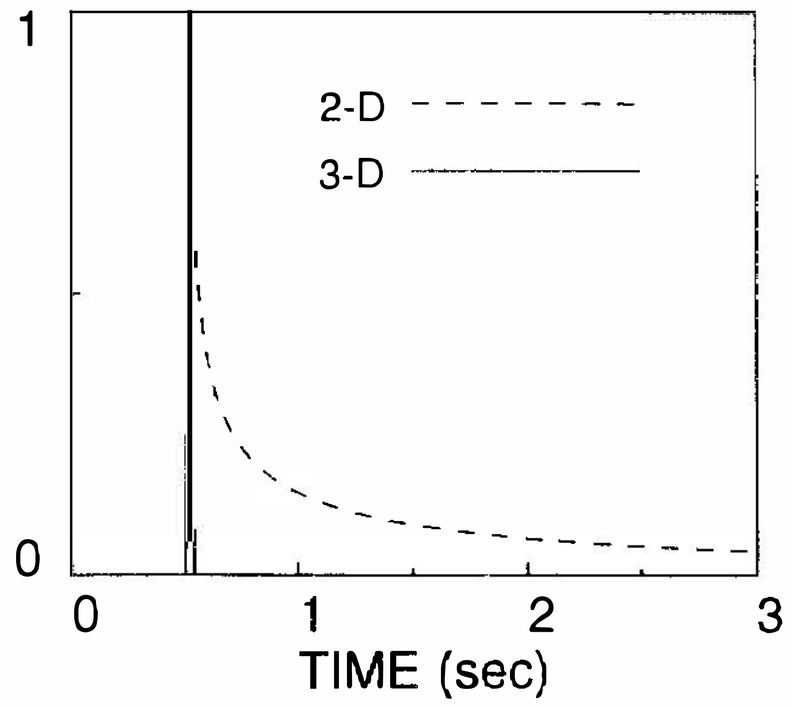

Fig. 1. Time histories of the 2-D and 3-D analytic Green's functions as shown in equations (2) and (4). Herein, r=4 and c=8 are used.

2.2 Point Source Expressions for the 2-D Green's Function

Following the derivation of the GRT and being solved by the Cagniard-de Hoop technique (Helmberger, 1983), the displacement potential of the point source, ϕ_p, in a whole-space can be expressed as:

$$\phi_p(r,z,t) = \sqrt{\frac{2}{r}}\frac{1}{\pi}\left[\frac{1}{\sqrt{t}} * J(t)\right], \tag{5}$$

where r and z are the radial and vertical coordinates, respectively, and

$$J(t) = \mathrm{Im}\left[\frac{\sqrt{p}}{\eta}\frac{dp}{dt}\right], \tag{6}$$

where p is the ray parameter, and $\eta = (1/c^2 - p^2)$. Im represents the image part of a complex variable. However, from the work of Gilbert and Knopoff (1961), the solution for the line source, ϕ_L, excitation can be expressed as:

$$\phi_L(t,z,t) = \mathrm{Im}\left(\frac{1}{\eta}\frac{dp}{dt}\right), \tag{7}$$

or more explicitly

$$\phi_L = \frac{H(t - r/c)}{\sqrt{t^2 - r^2/c^2}}. \tag{8}$$

Thus, the point source solution (ϕ_p) represented from the line source solution *J(t)* in equation (6) as J=($\sqrt{P}$) ϕ_L can be determined. This approach can be used to simulate the waveform of an earthquake using the 2-D numerical Green's functions.

2.3 Finite Element Formulation

The 2-D wave equation, equation (3), can be formulated as the following finite element equation for shear wave propagation

$$[M]\,[A] + [K]\,[D] = [F]\,, \tag{9}$$

where [*M*] is the global mass matrix, [*K*] the global stiffness matrix, [*A*] and [*D*], respectively, the vectors of the global acceleration and displacement of the model at grid points. [*F*] is the vector of the external loading forces at source points. To solve the temporal derivatives of equation (9) on each grid point, in this study, the second derivatives are introduced by the use of explicit finite difference approximation (Wylie, 1975), as follows:

$$\begin{aligned} [V(t+1/2\ \Delta t)] &= [V(t-1/2\ \Delta t)] + \Delta t[A(t)], \\ [D(t+\Delta t)] &= [D(t)] + \Delta t[V(t+1/2\ \Delta t)], \end{aligned} \tag{10}$$

where the definitions of *A* and *D* are the same as those in equation (9). *V* is the vector of the global velocity, and Δt is the time interval used in numerical integration. Thus, the displacement *D* on time $t + \Delta t$ is computed from the previous computed values of *D(t)*, *V(t* - 1/2 Δt) and *A(t)*. The finite element code development and mesh design are described in more detail in Huang (1989) and Huang and Yeh (1994).

2.4 Source Representation for Shear Dislocation Fault

Following the definition of Helmberger and Harkrider (1978), the tangential displacement U_{SH} can be expressed as:

$$U_{SH} = TSS\,A_4 + TDS\,A_5, \tag{11}$$

where *TSS* and *TDS* are the vertical tangential strike-slip and the dip-slip displacement Green's functions, respectively. Both A_4 and A_5 can be expressed as:

$$\begin{aligned} \mathrm{A}_4 &= \cos 2\theta\ \cos\lambda\ \sin\delta - 1/2\ \sin 2\theta\ \sin\lambda\ \sin 2\delta, \\ \mathrm{A}_5 &= \sin\theta\ \cos\lambda\ \cos\delta - \cos\theta\ \sin\lambda\ \cos 2\delta, \end{aligned} \tag{12}$$

where θ is the strike from the end of the fault, λ is the rake angle, and δ is the dip angle. To introduce the shear dislocation source to numerical modeling, Vidale *et al.* (1985) used the GRT to generate the displacements in a small ring around the source point. Those prescribed displacements drove the FD grids to simulate the Green's functions. In this study, the concept of equivalent body forces (Aki and Richards, 1980) was employed. The direct implementation of the couple of body forces on the source grids made the modeling of the explosion and shear dislocation sources successful, while simplifying the numerical computations.

3. RESULTS

3.1 Testing for the 3-D Green's Functions

Figure 2 shows the 2-D and 3-D numerical Green's functions of the whole space model with different epicentral distances. The 2-D synthetic seismograms show the same tail behavior as the analytic Green's function (Figure 1); however, the 3-D synthetic seismograms show the δ-function behavior except for some numerical errors from the inexact δ-type input source time function.

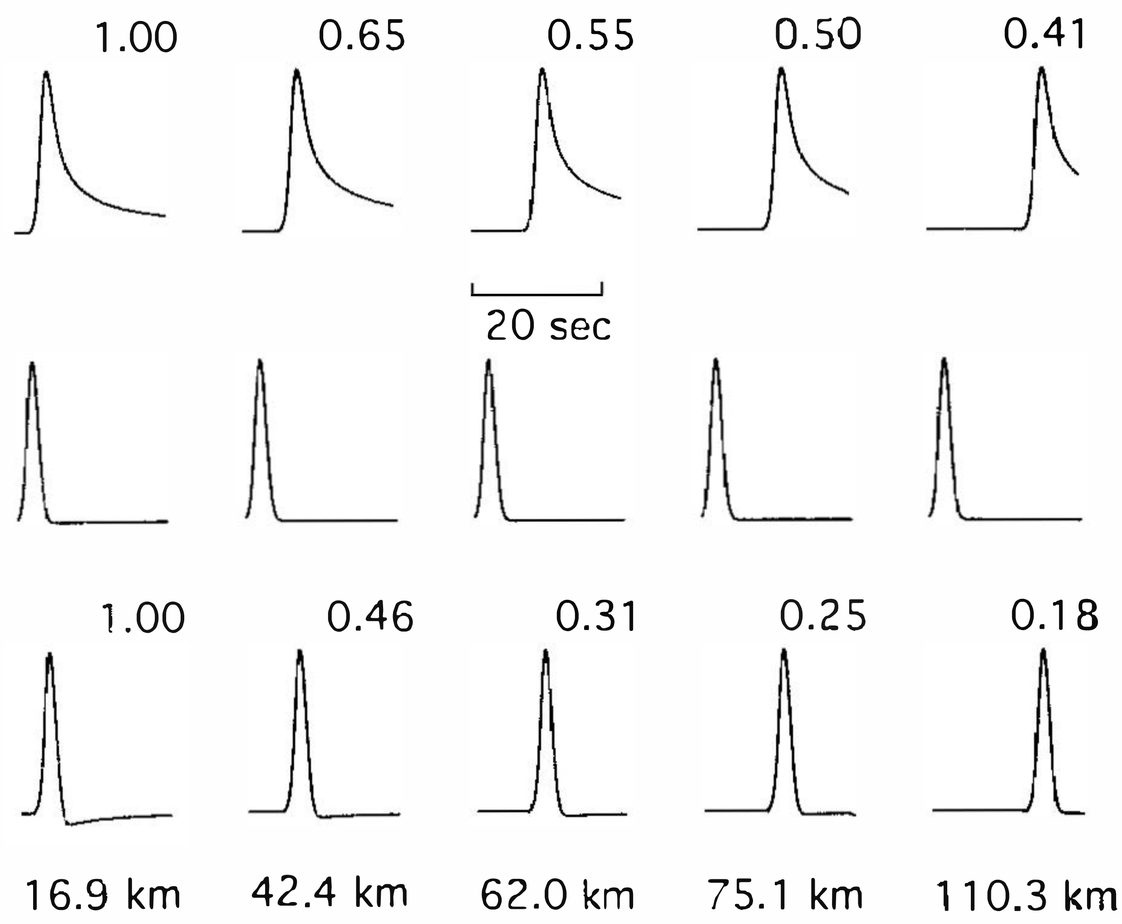

Fig. 2. Comparison of the seismograms of both the 2-D and 3-D numerical Green's functions in whole space. The time scale is the same for all seismograms and shown in the figure. The number in the bottom of each column is the distance between source and receivers. The seismograms in the upper row are the line source (2-D) Green's functions. Those in the middle row are the input source time functions. The lower row represents the corrected point source (3-D) Green's functions. The associated number with each plot represents the amplitude.

3.2 Comparison With Other Methods

To test the accuracy of this method, the results are compared with those from other methods. Herein, a model with one layer over a half-space that was well tested by the GRT (Apsel and Luco, 1983) is used for comparison. The TSS Green's functions of the shear dislocation fault are compared in Figure 3 and the TDS in Figure 4. Following the results of Vidale *et al.* (1985), the synthetics of this study are convoluted with the long-period WWSSN instrument response. The waveforms computed by the GRT, FD and FE of this study are close to each other. This indicates that the method proposed in this study is indeed suitable for modeling earthquake ground motions from lateral inhomogeneous models.

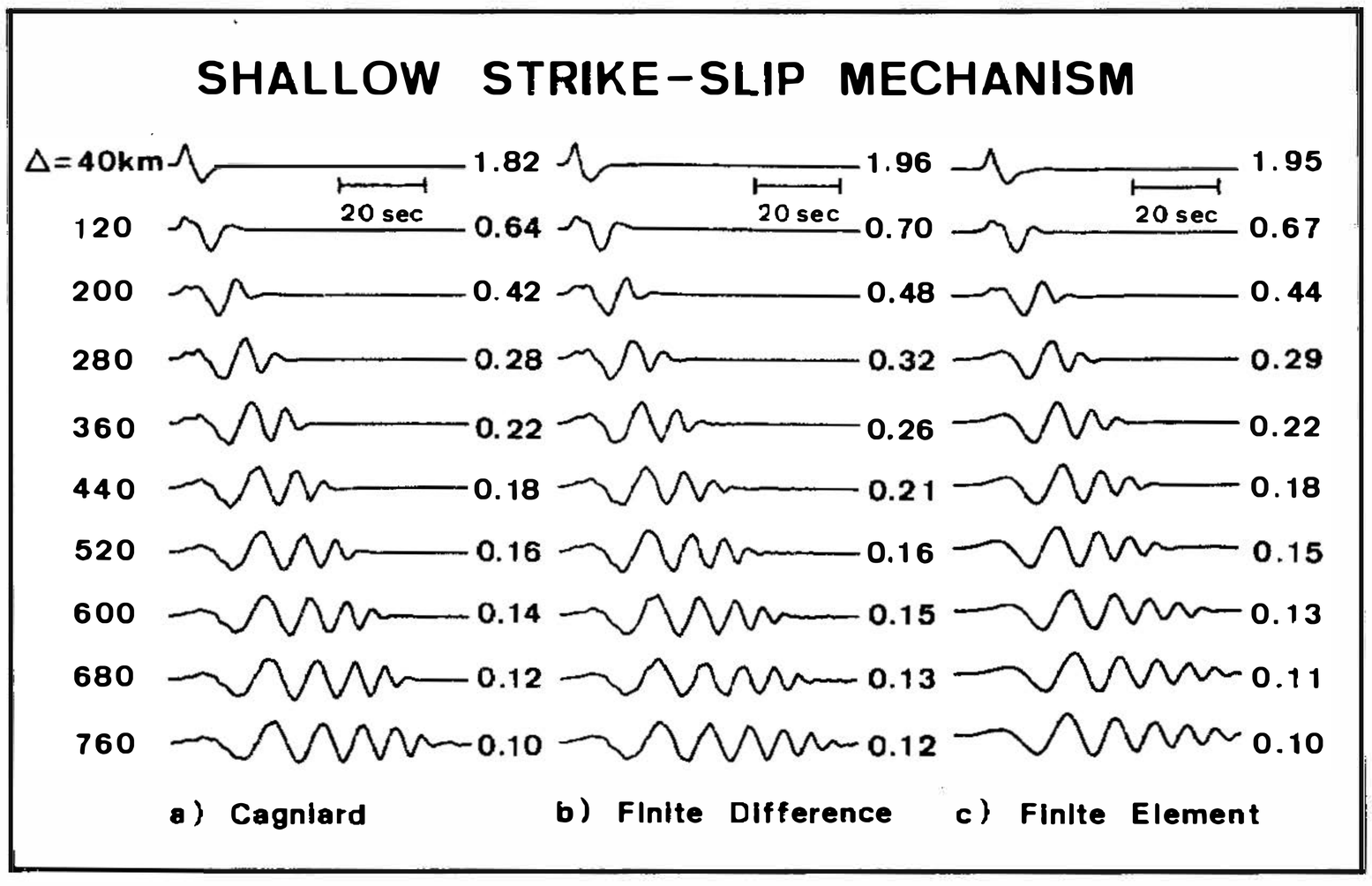

Fig. 3. Comparison of the synthetic seismograms computed by different methods; (a) the Cagniard-de Hoop method, (b) the finite difference Method (Vidale *et al.*, 1985), and (c) the finite element method of this study. The earth model is a one layer over half space structure as used by Vidale *et al.* (1995). The source mechanism is a point strike-slip fault on the upper layer. The synthetic seismograms of columns (a) and (b) are from Vidale *et al.* (1985).

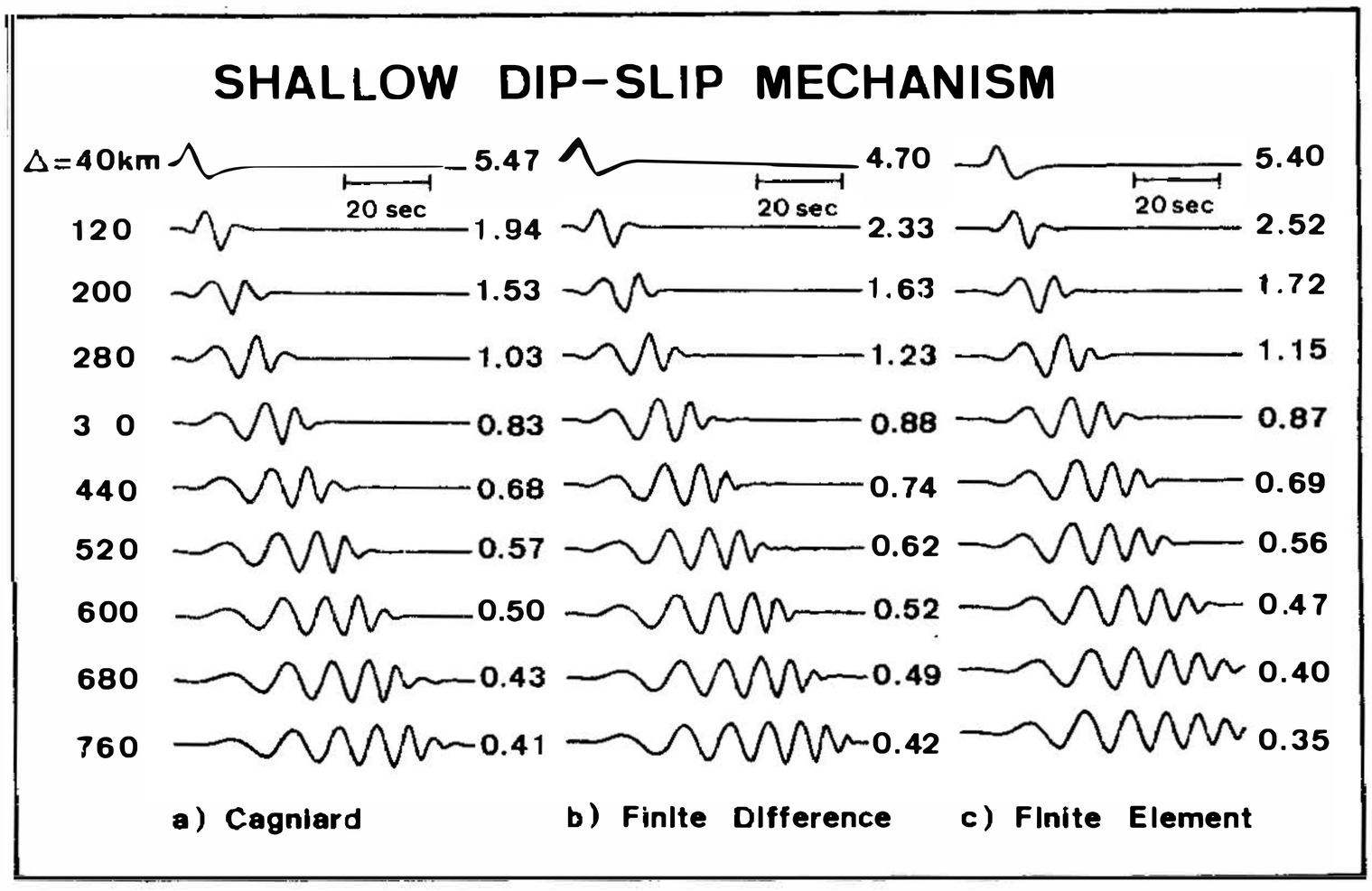

Fig. 4. Comparison of the synthetic seismograms computed by different methods. All definitions are the same as those in Figure 3. The seismograms of this figure were computed from a point source with dip-slip fault mechanism.

3.3 Point Source Snapshots Modification

Figure 5a shows the synthetic SH-wave displacement seismograms from a pure strike-slip point source on a lateral inhomogeneous earth model (Figure 5b). The recording sites are on a free surface and are indicated as open triangle signs in Figure 5b. It is found that the lateral phases of seismograms are strongly distorted by the embedded 2-D structure. The features of these seismograms are their long duration on the right of the source and the complex waveforms on the left. To clearly interpret the interaction of a complex earth model and seismic wavefield, usually, the examination of wave fields in space (i.e. snapshots) is necessary. However, no exact point source snapshots have been discussed previously. To calibrate the waveform and amplitude of the numerical point source Green's function as shown in equation (5), a convolution is necessary for the 2-D Green's function *(J(t))*. However, it is very difficult to apply the above technique for the calibration of the line source wave fields over all spatial grid points because all snapshots of the 2-D model on every time step are necessary. Those data are hard to store in present-day computers. Fortunately, to verify the wave fields variations in space, it is unnecessary to check such snapshots on every time step. Usually, only some snapshots separated in time are selected. Herein, the correction of the line source snapshot to the point source snapshot was accomplished according to the following approach. For snapshots selected in a defined time step (t_0), the convolution of $1/(\sqrt{t})$ of equation (5) in spatial domain can be implemented by the integration of the line source time histories at each grid point with the folding $1/(\sqrt{t})$ which was initiated at t_0. The corrected snapshot was obtained following the computation of wave propagation step by step till t_0. In the real case, the corrected snapshots may be the by-product of the main computation. The successfulness of this calibration is demonstrated by a band limited δ-function propagating in the whole space as shown in Figure 6. The Heaviside step type tail of the line source snapshot has effectively been corrected in the point source snapshot. In complex earth models, the variation becomes more complex than that in Figure 6. Figure 7 is the color display of the point source snapshot at time 48 sec after a pure dip-slip fault rupture of the model (Figure 5b). Comparing Figure 7 with its line source response (Figure 8), it is found that although the travel time of snapshots from both the line and point source is the same, the energy distribution is different. Again, the Heaviside step type tail of line source snapshot has effectively been corrected in the point source snapshot. Only the point source snapshot represented the true amplitude of the wavefield in space.

4. DISCUSSION

The FE approach with the line to point source transform has been shown to successfully model the SH waveforms. A numerical test of this method against an analytical method and the FDM shows a good agreement. The major advantage of this method is that the model can have arbitrary velocity and density variations, including dipping and curve boundaries, velocity and density gradients, and a low-velocity zone. The mesh design for the FE numerical grids can be irregular. The FE model can effectively be defined as fine grids in a low velocity zone or shallow layers with high velocity gradients, and therefore be defined as coarse grids in high velocity areas. However, such changed grid sizes are not allowed by the FD method. Employ-

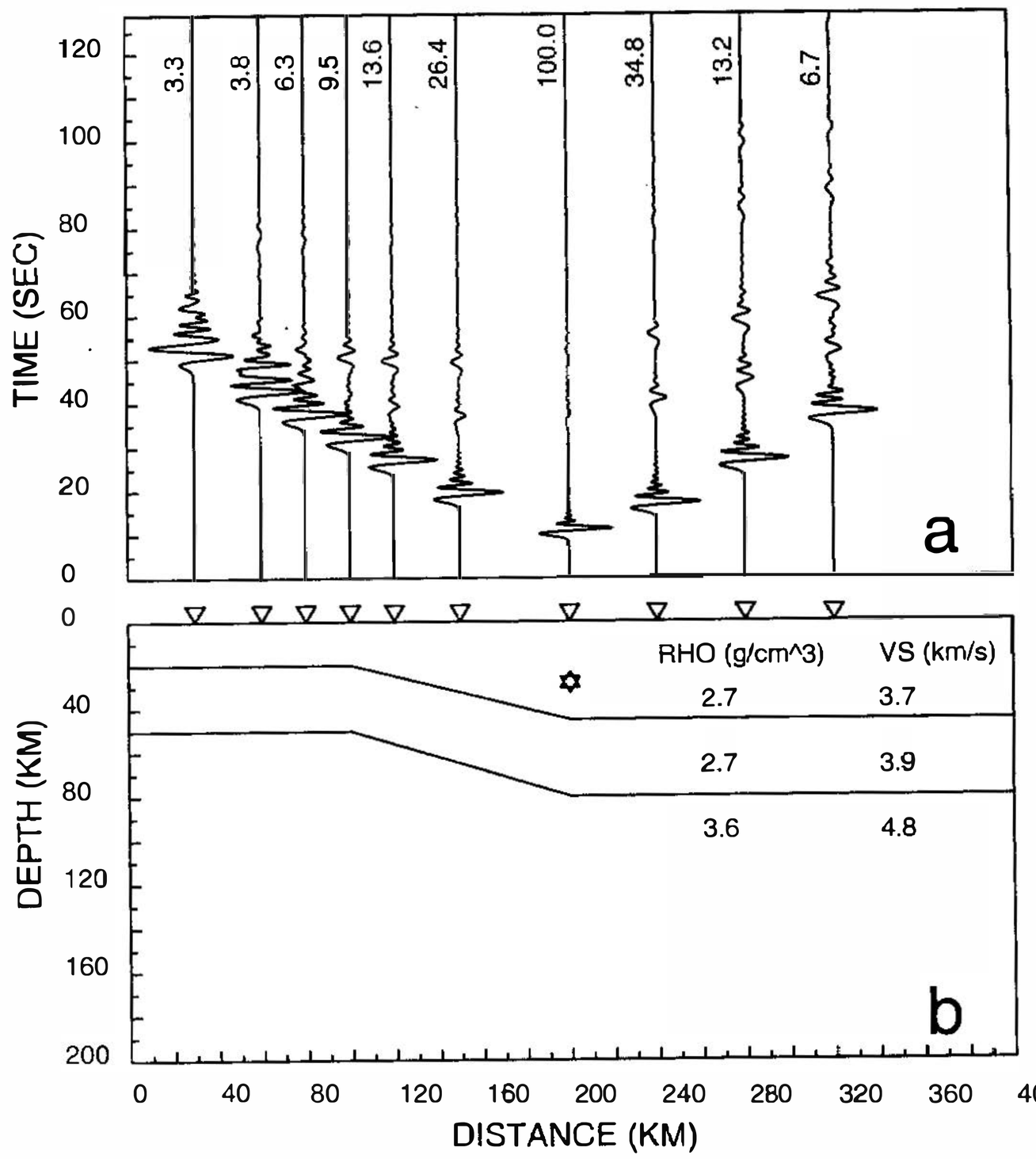

Fig. 5. (a) The seismic profile of a point source with dip-slip mechanism. The number at the end of each seismogram represents its normalized amplitude. (b) A lateral inhomogeneous model used to compute the seismic profile of Figure 5 (a). The star sign shows the location of the source. The triangle signs are the receivers on free surface. The density and shear velocity are denoted as RHO and VS.

ing this method to propagate earthquake energy, the path effects can be computed for the complex earth model in different scales. The application of this approach may be contributed to strong ground motion modeling for shallow structure amplification, determining source parameters in regional distance using broad band seismograms and studying slab structure at teleseismic distance. The extension to model the P-SV case is straightforward and is easily modified based on this study. The major disadvantages of this approach are that the computations take too much time to propagate earthquake energy numerically and the nature of the high frequency results is limited. Usually, the grid size constraints the highest frequency which is allowed. Furthermore, the model must be two-dimensional. In principle, the third dimension, which is perpendicular to the model, should be considered as an infinite extension.

The potential applications of this method to earthquake study in the Taiwan area extend into several branches. First, newly deployed strong motion instruments in the wide area of Taiwan provide an excellent data set to study strong motion amplification in shallow basins as

well as the topographic effects in the Central Mountain Range. Second, modeling seismograms from the Taiwan east-west cross section may provide important information of the deep structures. Third, constructing the lateral inhomogeneous Green's functions data bank of the Taiwan area by this FE approach provides accurate source parameter estimations in regional distance using the broad-band seismograms.

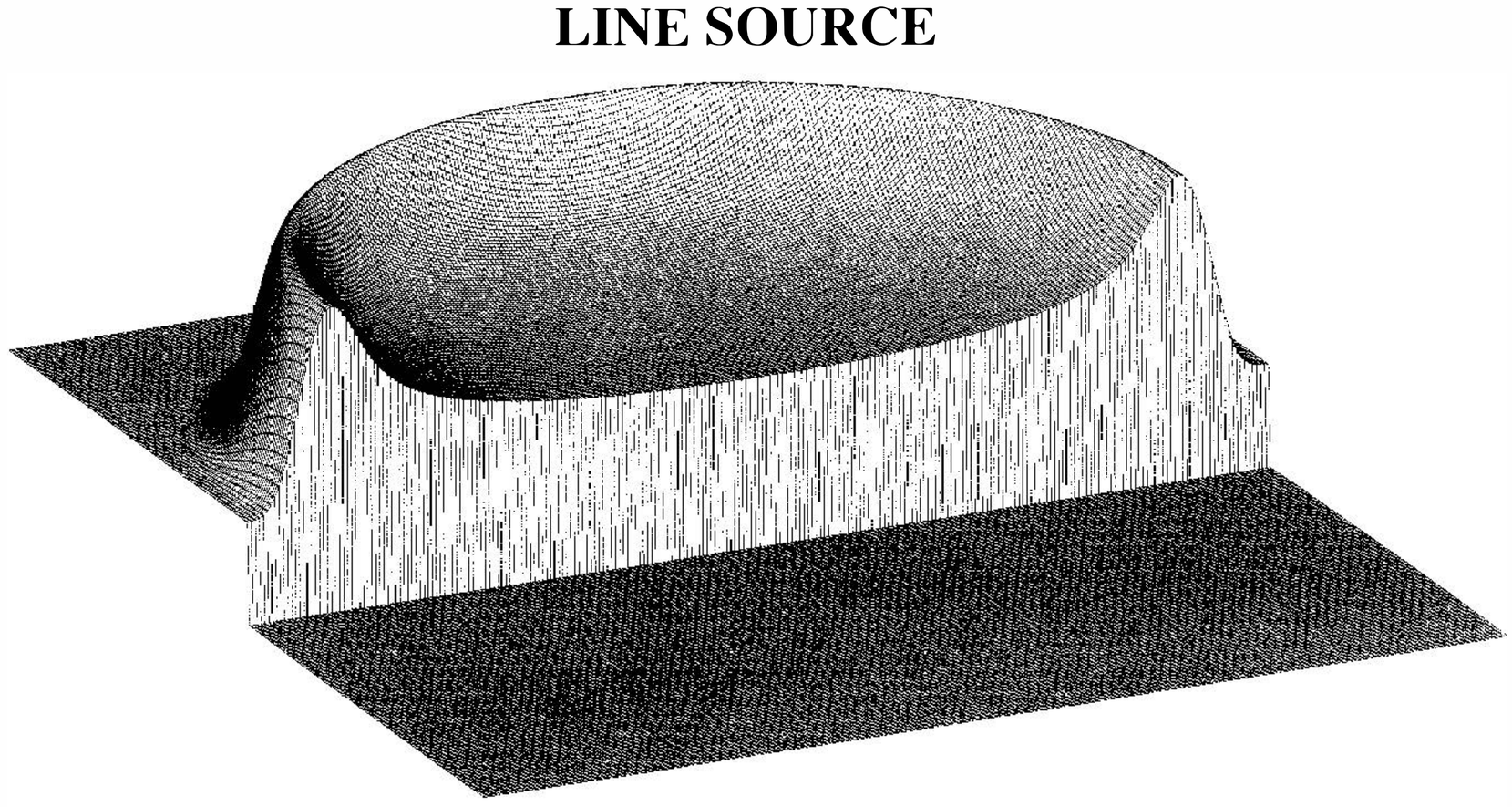

Fig. 6. Snapshot of the line source response (2-D) and its point source correction (3-D) in whole space. The input source is a band limited δ-function as shown in Figure 2 with the explosive type source mechanism. Two horizontal components define the model and a vertical component represents the wavefield amplitude. For the symmetry of the wavefields, the amplitudes of half model on the front side are muted.

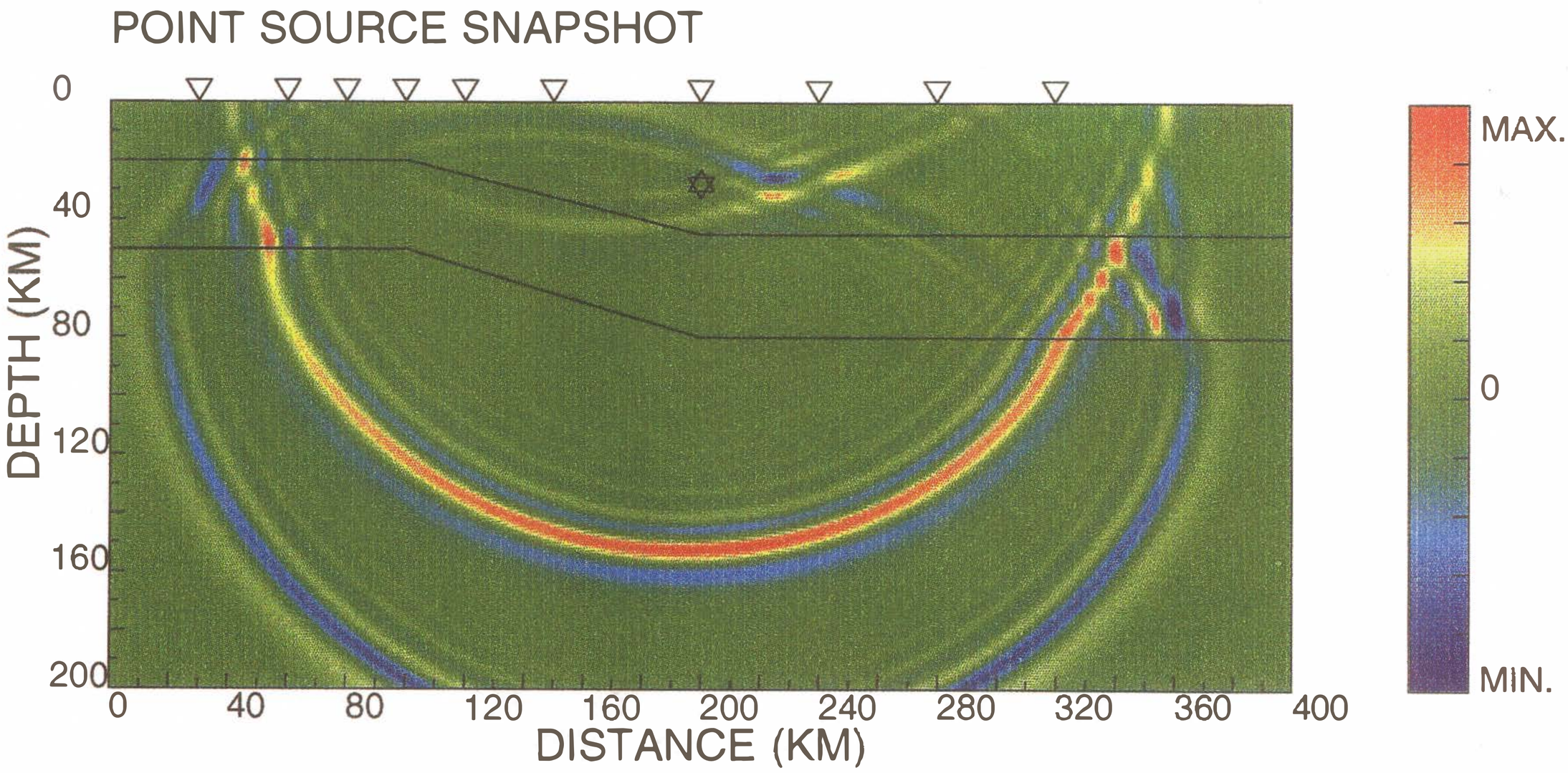

Fig. 7. The seismic energy distribution for the case of Figure 5 after 48 seconds from source rupture. The amplitude at each grid point of the model has been corrected as a point source radiation using the method proposed in this study. The amplitudes of the grid points of this snapshot are normalized based on the color tape on the right hand side of this figure. The model definition is the same as in Figure 5.

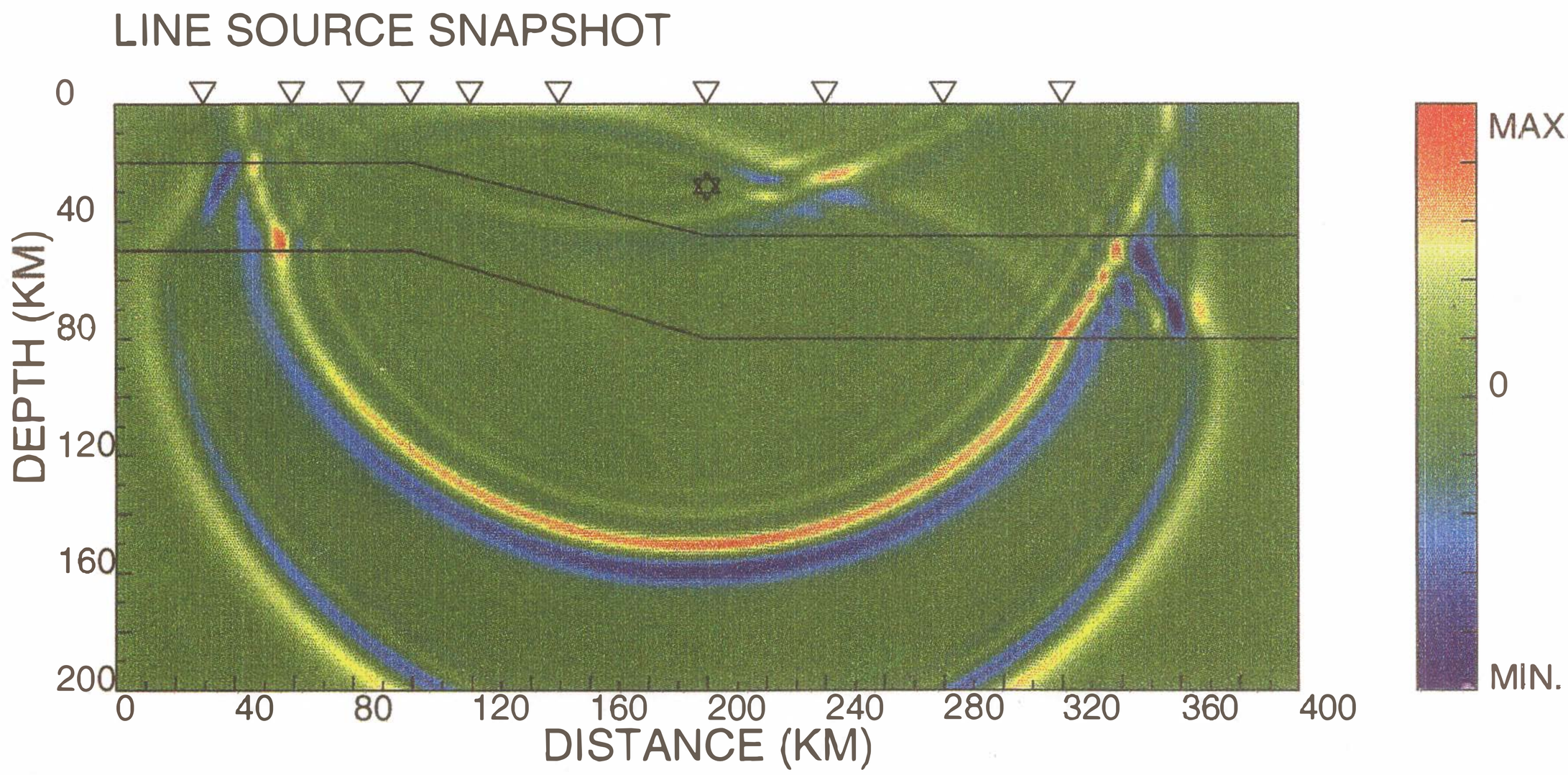

Fig. 8. The snapshot of the line source response of Figure 7. The amplitudes of the grid points of this snapshot are normalized based on the peak value of this snapshot.

5. CONCLUSIONS

A new method to numerically synthesize seismograms was proposed and well tested. This method is based on the equivalence body force concept, in which only suitable body forces are loaded on the source points of the finite element mesh, and no interface between source area and numerical model is needed. Furthermore, a simple method to calibrate the line source snapshots to point source was developed. These Green's functions are easily substituted for the standard Green's functions of the linear moment tensor inversion algorithms, but include 2-D structures. Potential applications of this method for seismological research in Taiwan have also been proposed.

Acknowledgments The author would like to express his special thanks to D. V. Helmberger and H. Kanamori for valuable discussion. This research was supported by Academia Sinica and the National Science Council of the Republic of China under grants NSC 82-0202-M-001-098, NSC 83-0202-M-001-040 and NSC 84-2111-M-001-008.

REFERENCES

Aki, K., and K. L. Larner, 1970: Surface motion of a layered medium having an irregular interface due to incident plane SH waves. *J. Geophys. Res.*, **75**, 933-954.

Aki, K., and P. G. Richards, 1980: Quantitative Seismology: Theory and Methods. Freeman, San Francisco, California, 932pp.

Apsel, R. J., and J. E. Luco, 1983: On the Green's functions for a layered halfspace. *Bull. Seis. Soc. Am.*, **73**, 909-925.

Chapman, C. H., 1978: A new method for computing synthetic seismograms. *Geophys. J.*, **54**, 481-518.

Dravinski, M., 1983: Scattering of plane harmonic SH waves by dipping layers of arbitrary shape. *Bull. Seis. Soc. Am.*, **73**, 1309-1319.

Gilbert, F., and L. Knopoff, 1961: The directivity problem for a buried line source. *Geophysics*, **26**, 626-634.

Heaton, T. H., and D. V. Helmberger, 1977: A study of the strong ground motion of the Borrego Mountain, California, earthquake. *Bull. Seis. Soc. Am.*, **67**, 315-330.

Helmberger, D. V., 1983: Theory and application of synthetic seismograms, In: H. Kanamori and E. Boschi (Eds.), Earthquakes: Observations, Theory and Interpretation, Proc. Int. Sch. Phys. Course LXXXV, 174-221.

Helmberger, D. V., and D. G. Harkrider, 1978: Modeling earthquakes with ray theory, In; J. Miklowitz and J. D. Achenbach (Eds.), Modern Problems in Elastic Wave Propagation, John Wiley and Sons, New York, 499-518.

Ho-Liu, P., and D. V. Helmberger, 1989: Modeling regional Love waves; Imperial Valley to Pasadena. *Bull. Seis. Soc. Am.*, **79**, 1194-1209.

Huang, B. S., 1989: Modeling seismic source geometry and rupture processes by the finite element method. Ph. D. Thesis, National Central Univ., 136pp.

Huang, B. S., 1994: Estimation of source parameters by the inversion of near source strong motion wave forms. *TAO*, **5**, 11-26.

Huang, B. S., and Y. T. Yeh, 1994: Near-source ground motion of a propagating rupture fault from the finite element modeling,. *TAO*, **5**, 295-311.

Kikuchi, K., and H. Kanamori, 1991: Inversion of complex body waves-III. *Bull. Seis. Soc. Am.*, **81**, 2335-2350.

Stump, B. W., and L. R. Johnson, 1977: The determination of source properties by the linear inversion of seismograms. *Bull. Seis. Soc. Am.*, **67**, 1489-1502.

Vidale, J. E., D. J. Helmberger, and R. W. Clayton, 1985: Finite-difference seismograms for SH waves. *Bull. Seis. Soc. Am.*, **75**, 1765-1782.

Wang, C. Y., and R. B. Herrmann, 1980: A numerical study of P-, SV-, and SH-wave generation in a plane layered medium. *Bull. Seis. Soc. Am.*, **70**, 1015-1036.

Wylie, C. R., 1975: Advanced Engineering Mathematics. McGraw-Hill, Inc, 937pp.